

**Fingering dynamics driven by a precipitation reaction: Nonlinear simulations**Priyanka Shukla<sup>1,2,\*</sup> and A. De Wit<sup>1,†</sup><sup>1</sup>*Université libre de Bruxelles (ULB), Nonlinear Physical Chemistry Unit, CP 231, Faculté des Sciences, Campus Plaine, 1050 Brussels, Belgium*<sup>2</sup>*Department of Mathematics, Indian Institute of Technology Madras, Chennai 600036, India*

(Received 30 May 2015; revised manuscript received 13 November 2015; published 3 February 2016)

A fingering instability can develop at the interface between two fluids when the more mobile fluid is injected into the less-mobile one. For example, viscous fingering appears when a less viscous (i.e., more mobile) fluid displaces a more viscous (and hence less mobile) one in a porous medium. Fingering can also be due to a local change in mobility arising when a precipitation reaction locally decreases the permeability. We numerically analyze the properties of the related precipitation fingering patterns occurring when an  $A + B \rightarrow C$  chemical reaction takes place, where  $A$  and  $B$  are reactants in solution and  $C$  is a solid product. We show that, similarly to reactive viscous fingering patterns, the precipitation fingering structures differ depending on whether  $A$  invades  $B$  or vice versa. This asymmetry can be related to underlying asymmetric concentration profiles developing when diffusion coefficients or initial concentrations of the reactants differ. In contrast to reactive viscous fingering, however, precipitation fingering patterns appear at shorter time scales than viscous fingers because the solid product  $C$  has a diffusivity tending to zero which destabilizes the displacement. Moreover, contrary to reactive viscous fingering, the system is more unstable with regard to precipitation fingering when the high-concentrated solution is injected into the low-concentrated one or when the faster diffusing reactant displaces the slower diffusing one.

DOI: [10.1103/PhysRevE.93.023103](https://doi.org/10.1103/PhysRevE.93.023103)**I. INTRODUCTION**

A hydrodynamic fingering instability can arise at the interface of two solutions because of differences in physical properties, for instance, viscosity, density, surface tension, or permeability across the interface [1–4]. The interface deforms then into finger-shaped patterns frequently encountered in geochemical processes such as enhanced oil recovery, environmental remediation, CO<sub>2</sub> sequestration, hydrology, etc. [4–6]. Fingering emerges typically when the mobility decreases in the direction of the flow and this occurs in both miscible and immiscible systems. This is, for instance, the case when a less viscous, more mobile fluid displaces a more viscous and hence less mobile one in a porous medium, giving rise to viscous fingering (VF). Over the past few decades, viscous fingering has been studied extensively in both nonreactive [4,7–9] and reactive [10–20] systems from both experimental and theoretical points of view. Mobility gradients can also develop because of permeability gradients leading to fingering, for instance because of porous matrix dissolution [21–26]. In these reactive dissolution instabilities, an invading solution of a given chemical reactant dissolves the porous matrix which increases the porosity of the porous medium behind the moving interface. This increase in porosity leads to a situation where the region of higher permeability (and hence higher mobility) displaces the lower permeability (and hence lower mobility) zone, which triggers a fingering instability.

In the reverse situation of a traveling precipitation front, the interface is expected to be stable because precipitation decreases the permeability behind the front such that the gradient of mobility is stabilizing. Nevertheless, Nagatsu *et al.* [27]

have recently shown that a localized precipitation reaction induced by a simple  $A + B \rightarrow C$  reaction when a solution of  $A$  invades a solution of  $B$  with  $C$  being the solid product can trigger fingering in the zone where the more mobile solution of  $A$  displaces the less mobile precipitate  $C$ . A wealth of various precipitation patterns can then be obtained [27–31]. This precipitation-driven fingering is of interest due to its applications in CO<sub>2</sub> sequestration and mineralization [32,33], a process by which CO<sub>2</sub> dissolved in water reacts with ions such as Ca<sup>2+</sup> and forms precipitates mostly carbonates, which is useful for safe storage of CO<sub>2</sub> in underground reservoirs [5]. Nagatsu *et al.* [34] also experimentally investigated the effects of a precipitation reaction on miscible viscous fingering patterns in a Hele-Shaw cell. They found that the fingering dynamics depends on the amount of precipitate and on the ratio of the reactants concentration. Precipitation-driven fingering can occur even at the interface between two aqueous solutions of same viscosity because of a local decrease in mobility along the displacement direction [27–29]. The model of this precipitation-driven fingering bears analogies with the one of reactive viscous fingering [15–18] in the sense that fingering appears in both cases in a local region of negative gradient of mobility formed by the reaction along the flow direction. The negative gradient of mobility in reactive VF is due to the changes in viscosity by reaction, whereas in precipitation-driven fingering, it is due to a local change in permeability of the porous medium. In both cases also, the fingering patterns have been shown to be asymmetric whether  $A$  is injected into  $B$  or vice versa, a difference that can be understood in terms of asymmetric underlying concentration profiles when the initial concentrations of the reactants or their diffusion coefficients differ [15,27,30]. Thus, mathematically speaking, precipitation-driven fingering and reactive VF are described by similar reaction-diffusion-convection (RDC) models in which

\*priyanka@iitm.ac.in

†adewit@ulb.ac.be

the mobility  $M = \kappa/\mu$  is a function of the concentration of the product  $C$  of the reaction, with  $\kappa$  and  $\mu$  being the permeability and viscosity, respectively.

Although reactive VF has been well studied [10–20], the properties of precipitation-driven fingering are less understood. In the case of precipitation, the solid product can barely diffuse, which differs considerably from reactive VF in which the reactants  $A$  and  $B$  and the product  $C$  can have diffusion coefficients of the same order of magnitude. Whether this slow diffusivity of the precipitation product  $C$  affects the physical and statistical properties of precipitation patterns is still unclear.

In this context, the objective of the present study is to investigate numerically the characteristics of precipitation-driven fingering patterns and to compare them with those of reactive VF patterns [15] and in particular to investigate the influence of the fact that the precipitate does not diffuse much. In order to do so, the RDC model of precipitation-driven fingering [27] is modified to allow the diffusivity of the solid product to tend to zero. We show that this slow diffusivity of the precipitate has important consequences on the fingering patterns, including much earlier destabilization and smaller wavelength.

This paper is organized as follows. The problem description and the related RDC model are given in Sec. II. In Sec. II B, the numerical method used to integrate the model is discussed. The characteristics of precipitation fingering patterns and in particular the influence of the diffusivity of the solid product are studied in Sec. III. A parametric study is carried out in Sec. IV. The effect on asymmetry of precipitation fingering patterns, whether  $A$  invades  $B$  or vice versa, of varying the ratio of initial reactant concentration and diffusivity of reactant  $B$  is explained in Secs. IV C and IV B, respectively. At the end, conclusions are given in Sec. VI.

## II. PROBLEM DESCRIPTION AND GOVERNING EQUATIONS

We consider a homogeneous two-dimensional porous medium or a horizontal thin Hele-Shaw cell, of length  $L_x$  and width  $L_y$  with initial permeability  $\kappa_0$ , as depicted schematically in Fig. 1. In this system, a solution of reactant  $B$  in initial concentration  $b_0$  is sandwiched between solutions of reactant  $A$  with concentration  $a_0$  ( $a_0 \leq b_0$ ). We assume that the viscosity  $\mu$  and density  $\rho$  of the two solutions are equal and constant. Such an initial configuration allows us to study two cases—namely when  $A$  invades  $B$  and vice versa—simultaneously in one single numerical simulation. The initial positions of the left and right miscible interfaces, where  $A$  and  $B$  come into contact and react, are  $x_l$  and  $x_r$ , respectively. The solutions are displaced from left to right at a constant speed  $U$  such that the solution  $A$  displaces the solution  $B$  at  $x = x_l$  while the solution  $A$  is being displaced by the solution  $B$  at  $x = x_r$ . A precipitation reaction of type  $A + B \rightarrow C$  takes place at the miscible interfaces producing a solid product  $C$  in the reactive zone around the initial contact lines. This solid precipitate is present in the solution as small particles that can diffuse in the solvent with a low diffusivity  $D_C$  and be advected by the flow. Its concentration in the solvent is denoted by  $c$ .

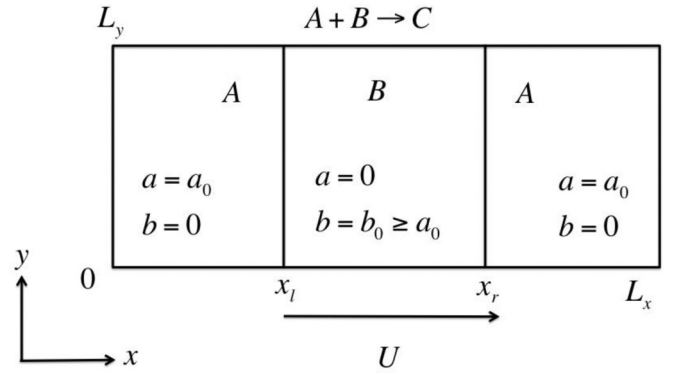


FIG. 1. Schematic diagram of a two-dimensional porous medium of dimensions  $L_x \times L_y$  with permeability  $\kappa_0$  in which a solution of reactant  $B$  sandwiched between the solutions of reactant  $A$  is displaced from left to right at a constant speed  $U$ .  $x_l$  and  $x_r$  are the initial positions of the left and the right miscible interfaces, respectively.

We assume here that the presence of the precipitate  $C$  does not change the density  $\rho$  and the viscosity  $\mu$  of the solvent, which are thus kept constant. Moreover, we assume that the porosity remains roughly constant and that the solid phase changes only substantially the permeability  $\kappa$  of the porous matrix. This simplifying assumption is motivated by the fact that there is no universal relation between permeability and porosity changes as the link between both quantities depends on evolution processes [35–38]. Therefore, for simplicity, we assume here that the porosity remains constant and that precipitation affects only the permeability. This is, for instance, the case if the precipitate is in small amounts and blocks preferentially small-sized connecting pores [39]. This can induce a negligible change of porosity while affecting much more drastically the permeability. More detailed studies of precipitation fingering in which both porosity and permeability [40,41] and potentially the density, viscosity, and diffusion coefficients are affected by the solid product of the reaction are left for the future.

In the present paper, we analyze thus the fingering instability which arises due to changes in the permeability  $\kappa$  of the porous medium by a precipitation reaction for a constant viscosity  $\mu$ , density  $\rho$ , and porosity  $\phi$ . Fingering develops locally in the zone where the reactant solution with reference permeability  $\kappa_0$  (or mobility  $M_0 = \kappa_0/\mu$ ) pushes the solution of the precipitate  $C$  of lower permeability (or lower mobility). The flow field, considered as incompressible (1), follows Darcy’s law (2) coupled to the evolution equations for the concentrations (3)–(5) via the permeability  $\kappa = \kappa(c)$  (6), which is a function of the local concentration  $c(x, y, t)$  of the product  $C$ . The resulting RDC model reads [10,11,15–18,27]:

$$\nabla \cdot \mathbf{u} = 0, \quad (1)$$

$$\nabla p = -\frac{\mu}{\kappa(c)} \mathbf{u}, \quad (2)$$

$$\frac{\partial a}{\partial t} + \mathbf{u} \cdot \nabla a = D_A \nabla^2 a - k a b, \quad (3)$$

$$\frac{\partial b}{\partial t} + \mathbf{u} \cdot \nabla b = D_B \nabla^2 b - k a b, \quad (4)$$

$$\frac{\partial c}{\partial t} + \mathbf{u} \cdot \nabla c = D_C \nabla^2 c + k a b, \quad (5)$$

where  $(a, D_A)$ ,  $(b, D_B)$ , and  $(c, D_C)$  denote the (concentration and diffusion coefficients) of species  $A$ ,  $B$ , and  $C$ , respectively;  $p$  is the pressure;  $\mathbf{u} = (u, v)$  is the two-dimensional velocity vector and  $k$  is the kinetic constant. By analogy with previous works on classical VF [7,8,42–45] or studies of rock dissolution [21,24,26] and reactive VF [15–18], the permeability of the system is assumed to be a decreasing function of the product concentration as [27]

$$\kappa(c) = \kappa_0 e^{-R(c/a_0)}, \quad (6)$$

where  $\kappa_0$  is the permeability when  $c = 0$ , i.e., in absence of any precipitate. Let  $\kappa_m = \kappa(a_0) = \kappa_0 e^{-R}$  be the permeability when  $c = a_0$ . The parameter  $R = \ln(M_0/M_m)$  is then defined as the log-mobility ratio where  $M_0 = \kappa_0/\mu$  and  $M_m = \kappa_m/\mu$  are the mobilities when  $c = 0$  and  $c = a_0$ , respectively. The parameter  $R$  quantifies the influence of precipitation on permeability changes. When  $R > 0$ , the precipitate  $C$  reduces the permeability of the porous matrix locally. A negative  $R$  could describe dissolution of the rock upon production of  $C$  but this will not be addressed here.

### A. Nondimensional equations

Mathematically, Eqs. (1)–(6) are similar to those describing reactive VF induced by an  $A + B \rightarrow C$  reaction changing the viscosity at a given constant  $\kappa$  [15–20]. The main difference between reactive and precipitation-driven fingering, however, is in the order of magnitude of the diffusion coefficients. In reactive VF, the reactants  $A$  and  $B$  and the product  $C$  have diffusion coefficients of the same order while in the precipitation case the product  $C$  barely moves, i.e.,  $D_C$  is small. To take this specificity into account, we use here the diffusivity  $D_A$  of the reactant  $A$  as a reference scale for diffusivity. The reference scales for velocity, time, length, concentration, permeability, and pressure are thus taken as  $U$ ,  $D_A/U^2$ ,  $D_A/U$ ,  $a_0$ ,  $\kappa_0$ , and  $\mu D_A/\kappa_0$ , respectively.

For simplicity, we write Eqs. (1)–(6) in a reference frame moving with velocity  $U$ , i.e., the flow direction  $x$  and flow velocity  $\mathbf{u}$  are transformed as  $x' = x - Ut$  and  $\mathbf{u}' = \mathbf{u} - U\mathbf{e}_x$ , respectively, with  $\mathbf{e}_x$  being the unit vector along the  $x$  direction. The dimensionless form of (1)–(6) in the moving frame becomes

$$\nabla \cdot \mathbf{u} = 0, \quad (7)$$

$$\nabla p = -\frac{1}{\kappa(c)}(\mathbf{u} + \mathbf{e}_x), \quad (8)$$

$$\frac{\partial a}{\partial t} + \mathbf{u} \cdot \nabla a = \nabla^2 a - D_a a b, \quad (9)$$

$$\frac{\partial b}{\partial t} + \mathbf{u} \cdot \nabla b = \delta_b \nabla^2 b - D_a a b, \quad (10)$$

$$\frac{\partial c}{\partial t} + \mathbf{u} \cdot \nabla c = \delta_c \nabla^2 c + D_a a b, \quad (11)$$

$$\kappa(c) = e^{-Rc}, \quad (12)$$

where  $D_a = D_A \kappa a_0 / U^2$  is the dimensionless Damköhler number which quantifies the ratio of the hydrodynamic time scale  $\tau_h = D_A / U^2$  to the chemical time scale  $\tau_c = 1 / \kappa a_0$  and  $\delta_b = D_B / D_A$  and  $\delta_c = D_C / D_A$  are the diffusion coefficient

ratios. Taking the curl of equation (8) and introducing the stream function  $\psi$  as  $u = \partial\psi/\partial y$  and  $v = -\partial\psi/\partial x$ , we get

$$\nabla^2 \psi = R(\psi_x c_x + \psi_y c_y + c_y), \quad (13)$$

$$a_t + a_x \psi_y - a_y \psi_x = \nabla^2 a - D_a a b, \quad (14)$$

$$b_t + b_x \psi_y - b_y \psi_x = \delta_b \nabla^2 b - D_a a b, \quad (15)$$

$$c_t + c_x \psi_y - c_y \psi_x = \delta_c \nabla^2 c + D_a a b. \quad (16)$$

Note that, when  $D_a = 0$ , we recover a model for nonreactive fingering similar to the one studied by Tan and Homsy [7] in which  $\mu(c) = 1/\kappa(c) = e^{Rc}$ . For  $\delta_c = 1$ , Eqs. (13) and (16) are indeed the same as Eqs. (29)–(31) of Tan and Homsy [7]. When  $D_a \neq 0$ , and  $\delta_b$  and  $\delta_c \sim O(1)$ , the model is similar to the one investigated previously for reactive VF instability [15–20]. In particular, we can recover the modeling of the specific case of a simple  $A + B \rightarrow C$  reaction when  $C$  is a solute changing the viscosity of the solution and the solution of  $A$  and  $B$  have the same viscosity [15]. Moreover, modulo a change of variable (see Appendix), we recover the precipitation fingering model studied by Nagatsu *et al.* [27]. The difference with that precious study is that here we focus on the case  $\delta_b \sim O(1)$  and  $\delta_c \rightarrow 0$  to analyze the fingering patterns due to the formation of a barely diffusing precipitate  $C$ . Interestingly, our precipitation model in which the permeability varies with concentration also bears similarities with a generalized model for two-phase Hele-Shaw flows [46], in which the mobility varies with saturation. Our results might thus also shed light on dynamics related to viscosity or permeability changes with saturation in two-phase flow systems.

The last term of concentration equations, (14)–(16), quantifies the reaction rate  $\mathcal{R}$  defined as:

$$\mathcal{R}(x, y, t) = D_a a(x, y, t) b(x, y, t). \quad (17)$$

The initial conditions for the stream function and product concentration are  $\psi(x, y) = 0$  and  $c(x, y) = 0$  for all  $(x, y)$ , respectively. For the initial condition of the concentrations, we use two back step functions centered at the two locations  $x_l$  and  $x_r$  between  $A$  and  $B$  (see Fig. 1) with a random noise being introduced at  $x_l$  and  $x_r$  [15]:

$$[a(x, y), b(x, y)] = \begin{cases} [1, 0] & \text{for } 0 \leq x < x_l \\ [\frac{1}{2}(1 + \zeta r), \frac{1}{2}(1 - \zeta r)\phi] & \text{for } x = x_l \\ [0, \phi] & \text{for } x_l < x < x_r, \\ [\frac{1}{2}(1 - \zeta r), \frac{1}{2}(1 + \zeta r)\phi] & \text{for } x = x_r \\ [0, 1] & \text{for } x_r < x < \text{Pe}' \end{cases} \quad (18)$$

for all  $0 \leq y < \text{Pe}$ , where  $\phi = b_0/a_0$  is the initial concentration ratio of solutions  $A$  and  $B$ ,  $r$  is a random number between 0 and 1, and  $\zeta$  is an amplitude of order  $10^{-2}$ . The Péclet numbers  $\text{Pe}' = UL_x/D_A$  and  $\text{Pe} = UL_y/D_A$  represent the dimensionless length and width of the numerical domain. While  $\text{Pe}$  controls the number of fingers along the transverse direction,  $\text{Pe}'$  fixes the maximum time of simulations. The

dynamics of reactive precipitation fingering depends on five parameters, namely,  $R$ ,  $D_a$ ,  $\delta_b$ ,  $\delta_c$ , and  $\phi$ .

**B. Numerical method**

To integrate Eqs. (13)–(16) numerically, we use a pseudospectral numerical scheme [7,10,11,15,47,48] with periodic boundary conditions along both directions. The physical domain  $Pe' \times Pe$  is taken to be  $256 \times 64$ . In order to handle sharp jumps in the initial conditions leading to Gibb’s phenomenon [7], we use a small spatial step  $dx = dy = 0.125$  (i.e.,  $2048 \times 512$  spectral modes) and time step  $dt = 0.0025$ . This choice of spatial and time steps satisfies the Courant-Friedrichs-Lewy (CFL) condition necessary for the numerical stability [47–49], i.e.,  $dt \leq \epsilon(dx)^2$ , where  $\epsilon$  is a numerical-scheme-dependent constant. We find that the numerical stability is difficult to achieve if  $\delta_c \rightarrow 0$ , and therefore we restrict our computation to  $\delta_c \geq 0.01$ . We checked that the spatial and temporal evolution of the fingering pattern remains unchanged with time and spatial steps refinement to confirm the convergence of numerical solutions. We have also verified that the numerical results are unchanged at a fixed  $Pe$  when  $Pe'$  is increased as long as the numerical domain is long enough for the fingers not to be affected by the periodicity of the initial condition.

We have validated our numerical code with the case when all species diffuse at the same rate ( $\delta_b = \delta_c = 1$ ) and  $R < 0$  for which results of reactive VF when a chemical reaction produces a more viscous product in between the two less viscous solutions are recovered [15,18]. We note that, in this case, the onset time at which fingering appears is much longer than in the present precipitation case because, as will be seen in Sec. III, when the diffusivity of the product is of the same order as that of the reactants, the onset time of fingering is large and the system is less unstable.

In Secs. III and IV, we study the effect of varying the parameters  $\delta_c$ ,  $\delta_b$ ,  $R$ ,  $D_a$ , and  $\phi$  on the fingering properties in the specific case of precipitation for which the solid product barely moves, i.e.,  $\delta_c \sim 0$ . In the following sections, the concentration fields (Figs. 2, 4, 8, and 12) are shown in a color scale between 0 and 1, with red and blue denoting the maximum and minimum values, respectively.

**III. REACTIVE PRECIPITATE FINGERING**

In the symmetric case, for which the reactants  $A$  and  $B$  have the same initial concentration ( $\phi = 1$ ) and diffusion coefficients ( $\delta_b = 1$ ), the concentrations of the product  $C$  and the reaction rates  $\mathcal{R}$  are shown in Fig. 2 for  $\delta_c = 0.01$ ,  $R = 2$ , and  $D_a = 1$  (see the Supplemental Material for a movie [50]). It is seen that, as time evolves,  $A$  and  $B$  meet, react, and are transformed through the reaction to a solid precipitate  $C$  in the reactive zone. This solid precipitate changes locally the permeability of the porous medium, and, hence, the mobility of the solution. Consequently, a situation arises where locally a high-mobility solution of  $A$  invades a low-mobility zone containing  $C$  which triggers the fingering instability, as shown in Fig. 2. The corresponding reaction rate shows that the reaction zone remains localized at the reactive front of the displacement and moves with it. In the course of time, less and less precipitate is formed and the fingers extend longitudinally with less interactions. The precipitate is left behind the moving reaction zone, which appears here at the fixed position of the initial contact line as the images are shown in a moving reference frame.

To understand the origin of precipitation fingering, it is instructive to analyze the underlying reaction-diffusion (RD) profiles of concentration for species  $A$ ,  $B$ , and  $C$ , and of the permeability  $\kappa = e^{-Rc}$ , for various values of  $\delta_c$ . As seen in Fig. 3, the concentration profiles and permeability preserve symmetry around the initial location of the interface for  $\phi = 1$  and  $\delta_b = 1$ . Thus, fingering patterns are the same at both interfaces (only one of them is shown in Fig. 2) and the cases where  $A$  invades  $B$  and vice versa are identical. Furthermore, the product concentration is maximum at the initial contact location and decreases rapidly around it, see Fig. 3(a). Consequently, the permeability (hence mobility) decreases rapidly along the flow direction and approaches a minimum value at the initial contact position, as shown in Fig. 3(b). The extreme value of the product concentration (maximum) and permeability (minimum) at the contact lines increases with decreasing  $\delta_c$ . This decrease in permeability and hence mobility is due to the formation of the precipitate and fingering appears locally in the region where the negative

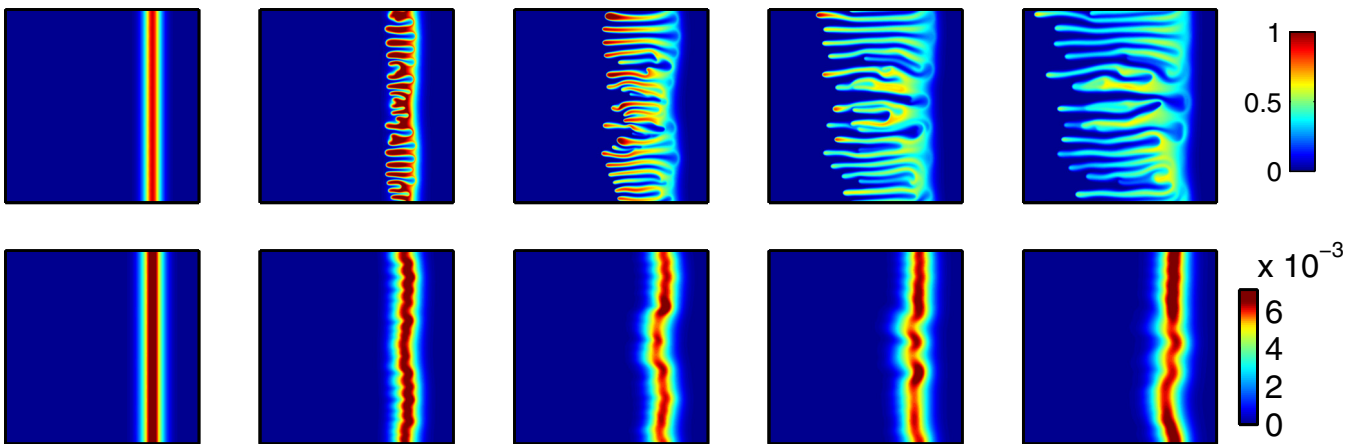


FIG. 2. Concentration of the product  $C$  (first row) and reaction rate  $\mathcal{R}$  (second row) for  $\delta_c = 0.01$ ,  $\delta_b = 1$ ,  $\phi = 1$ ,  $R = 2$ , and  $D_a = 1$ , at  $t = 20, 40, 60, 80$ , and  $100$  (from left to right).

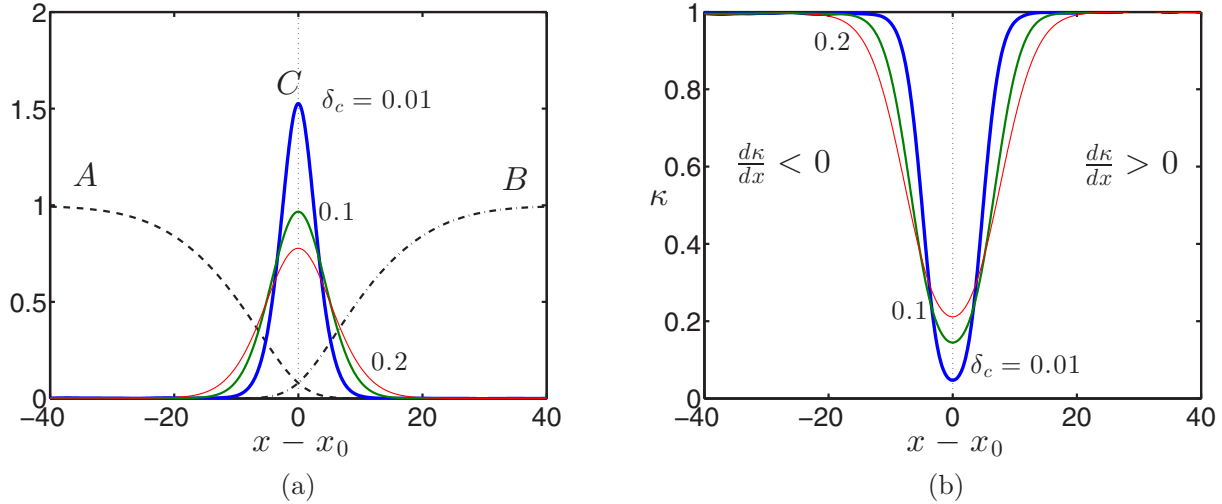


FIG. 3. Reaction-diffusion profiles for (a) concentrations and (b) permeability for three values of  $\delta_c$ : 0.01 (thickest blue line), 0.1 (thicker green line), and 0.2 (thick red line). Here the dashed, dash-dotted, and solid lines represent  $A$ ,  $B$ , and  $C$ , respectively. The initial location at  $x = x_l = x_r = x_0$  corresponds here to the black dotted line at origin. The other parameters are the same as those of Fig. 2.

permeability (hence mobility) gradient forms, i.e., where  $d\kappa/dx < 0$ . Figure 3(b) shows that, as  $\delta_c \rightarrow 0$ , the gradient  $d\kappa/dx$  becomes steeper, and therefore the system becomes more unstable, leading to quicker fingering instability as shown in Fig. 4.

Note that the precipitation fingering patterns differ from those of reactive VF [15] in the sense that (i) precipitation fingering appears at a constant viscosity and is due to the local change in permeability, (ii) the solid precipitate  $C$  diffuses very slowly as compared to other reactants, and (iii) the length and time scales for the appearance of precipitation-driven fingering are much smaller than for reactive VF.

**A. Effect of  $\delta_c$**

To see the effect of varying  $\delta_c$  on the nonlinear fingering pattern, the concentrations of the product are shown in Fig. 4 for  $\delta_c = 0.15, 0.10, 0.05$ , and  $0.01$ . The instability starts earlier and the number of fingers increases with decreasing  $\delta_c$ , i.e., the system becomes more unstable as  $\delta_c \rightarrow 0$ . This is related to the fact that the unfavorable gradient  $d\kappa/dx$  becomes steeper when  $\delta_c \rightarrow 0$ .

**B. Quantitative analysis**

To understand the dynamics of precipitation driven fingering, we perform a quantitative analysis by computing the transverse averaged profiles of various properties. To begin with, we calculate one-dimensional transverse averaged concentration and reaction rate profiles which are defined as

$$\langle c(x,t) \rangle = \frac{1}{L_y} \int_0^{L_y} c(x,y,t) dy \quad \text{and}$$

$$\langle \mathcal{R}(x,t) \rangle = \frac{1}{L_y} \int_0^{L_y} \mathcal{R}(x,y,t) dy, \quad (19)$$

respectively.

In absence of any mobility gradients ( $R = 0$ ), these profiles are equivalent to one-dimensional RD profiles. For the simulation of Fig. 2, the temporal evolution of transversely averaged profiles of concentrations of  $A$ ,  $B$ , and  $C$ , and reaction rate are shown in Fig. 5. Beyond the diffusion regime and when  $A$  and  $B$  start to react, the fingered precipitate starts to form in the reaction zone. As the system evolves in time, more and more precipitate is present which resists flow by decreasing locally the permeability. The transverse averaged profiles  $\langle c(x,t) \rangle$ , see Fig. 5(a), show that the concentration profiles are no longer smooth in the presence of fingering and feature characteristic bumps. The maximum of  $\langle c(x,t) \rangle$  decreases with time, which is due to the fact that the corresponding reaction rate  $\langle \mathcal{R}(x,t) \rangle$  decreases with time [see Fig. 5(b)] and that the precipitate is left behind the moving reaction front.

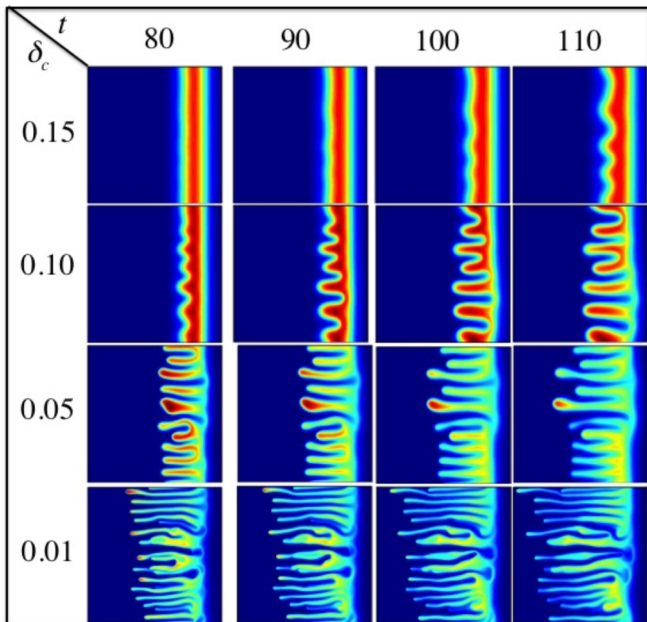


FIG. 4. Comparison of the concentrations of the product for decreasing values of  $\delta_c$  at  $t = 80, 90, 100$ , and  $110$ . The other parameters are the same as in Fig. 2.

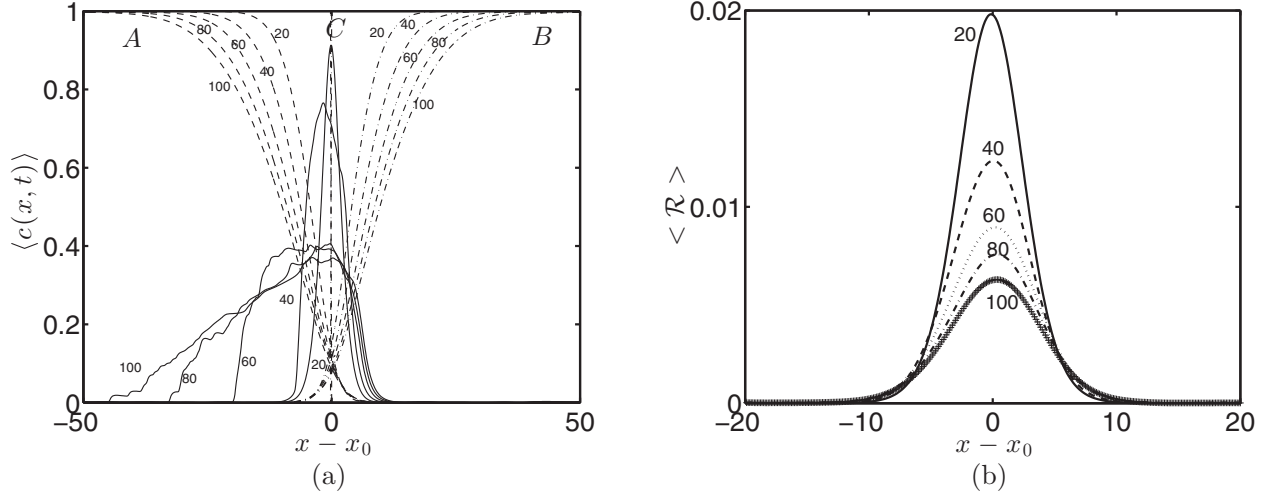


FIG. 5. Transverse averaged (a) concentration profiles of  $A$  (dashed line),  $B$  (dash-dotted line), and  $C$  (solid line), and (b) reaction rate profiles for the simulation of Fig. 2 at  $t = 0, 20, 40, 60, 80, 100$ . Here  $x_0$  is the initial location of the left interface  $x_l$ .

From transverse averaged profiles (19), one can next compute the mixing length  $L$  of the product  $C$  defined as the length of the zone where a precipitate is present, i.e., in which  $\langle c(x, t) \rangle$  is greater than 0.01 [15,51]. Figure 6 shows the variation of this mixing length with time for various values of  $\delta_c$ . In the diffusive regime, the mixing length follows a square root scaling with time, i.e.,  $L \propto \alpha \sqrt{t}$  where  $\alpha$  depends on the diffusivity of the reactants and product [52]. Gálfi and Rácz [52] showed that the width of the mixing zone depends on the reaction rate  $\mathcal{R}$ , (17), which is an implicit function of the permeability  $\kappa$ . Hence  $\mathcal{R}$  depends on the concentration of the product as well as the diffusivity ratio  $\delta_c$ . Thus, in the diffusive regime the mixing length depends on  $\delta_c$  (see inset of Fig. 6).

In the transition regime, the mixing length deviates from the diffusive  $\sqrt{t}$  scaling once the system enters into the convective regime for which the mixing length varies linearly with time. A kink, seen in the mixing length, represents the

time  $t = t_b$  beyond which the averaged concentration profiles  $\langle c(x, t) \rangle$  show a bumpy nature [see Fig. 5(a)]. Furthermore, by comparing Figs. 4 and 6 we see that, as  $\delta_c$  decreases, the system becomes more unstable and the onset time for fingering decreases.

### C. Statistical analysis

The moments of the transverse averaged profiles can be calculated as well [15,51,53]. The first moment, i.e., the center of mass  $m_c$  of the transverse averaged product concentration  $\langle c(x, t) \rangle$ , is defined as

$$m_c(t) = \int_0^{L_x} x g(x, t) dx, \quad (20)$$

where  $g(x, t) = \frac{\langle c(x, t) \rangle}{\int_0^{L_x} \langle c(x, t) \rangle dx}$  is the probability distribution function of  $\langle c(x, t) \rangle$ . A similar quantity can be computed for the reaction rate distribution to give its first moment  $m_R$ .

The temporal variation of the position of the first moment for the concentration  $m_c$  and reaction rate  $m_R$  are shown for various values of  $\delta_c$  in Figs. 7(a) and 7(b), respectively. It is seen in Fig. 7(a) that the center of mass of the concentration profiles  $m_c$  lags behind the reaction zone (i.e., moves backward in the moving frame). This is related to the fact that the precipitate fingers are left behind the reacting interface when it moves forward, see Figs. 4 and 5(a). This effect is enhanced when  $\delta_c$  is decreased. The center of mass of the reaction rate  $m_R$ , shown in Fig. 7(b), first moves backward and then forward along with back-and-forth motion, which is consistent with what we see in the reaction rate in Fig. 2. For  $\delta_c = 0.01$  [see the solid line in Fig. 7(b)],  $m_R$  first moves towards the left of the initial position of the interface until time  $t \sim 30$ , beyond which it travels to the right and eventually turns to the left at  $t \sim 85$ . This is due to the fact that when the convection is very strong it pushes reactants towards the forward (right) direction, and therefore  $m_R$  travels to the right where convection dominates, as shown in Fig. 7(b). By comparing  $m_R$  for various  $\delta_c$  we see that the time at which  $m_R$  travels towards the right decreases

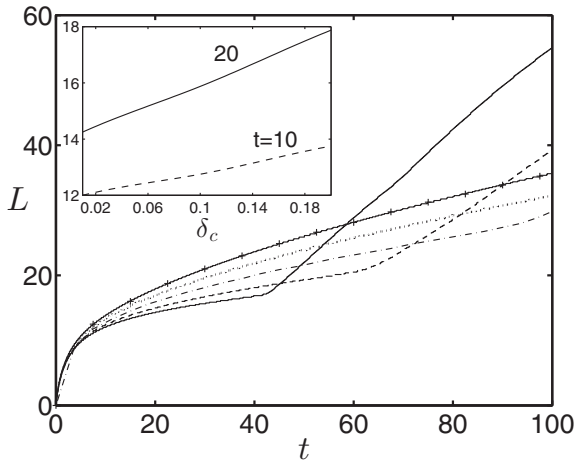


FIG. 6. Temporal variation of the mixing length  $L$  for various values of  $\delta_c = 0.01$  (solid line),  $0.05$  (dashed line),  $0.1$  (dash-dotted),  $0.15$  (dotted), and  $0.2$  (solid line with plus symbol). The inset shows the variation of  $L$  with  $\delta_c$  for two values of  $t = 10$  and  $20$ . Other parameters are the same as in Fig. 2.

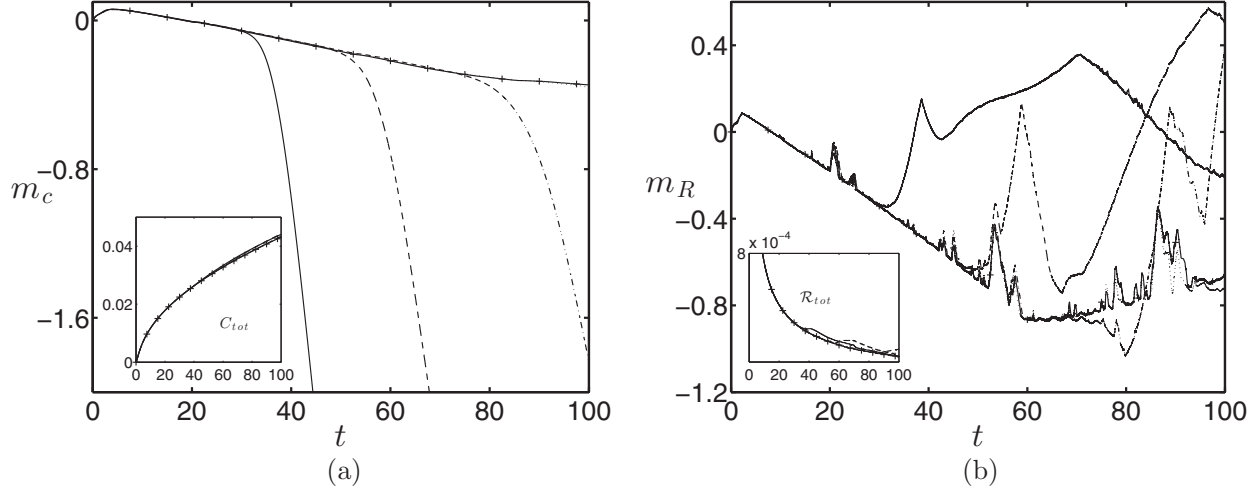


FIG. 7. Temporal variation of the center of mass for the (a) product  $m_c$  and (b) reaction rate  $m_R$  for various values of  $\delta_c$ . The insets of panel (a) and panel (b) show the corresponding variation of total concentration of the product,  $C_{\text{tot}}$ , and reaction rate,  $\mathcal{R}_{\text{tot}}$ , respectively. Parameters and line conventions are the same as those of Fig. 6.

with  $\delta_c$ , which means that the system is more unstable as convection starts earlier for decreasing  $\delta_c$ .

The overall yield of the precipitate formation can be determined by calculating the total precipitation amount  $C_{\text{tot}}$  and the total reaction rate  $\mathcal{R}_{\text{tot}}$  within the domain of interest, as defined below:

$$C_{\text{tot}}^l = \int_0^{L_y} \int_0^{L_x/2} c(x, y, t) dx dy,$$

$$\mathcal{R}_{\text{tot}}^l = \int_0^{L_y} \int_0^{L_x/2} \mathcal{R}(x, y, t) dx dy, \quad (21)$$

$$C_{\text{tot}}^r = \int_0^{L_y} \int_{L_x/2}^{L_x} c(x, y, t) dx dy,$$

$$\mathcal{R}_{\text{tot}}^r = \int_0^{L_y} \int_{L_x/2}^{L_x} \mathcal{R}(x, y, t) dx dy, \quad (22)$$

where the superscript  $l$  and  $r$  denote the left and right initial positions of interfaces, respectively. Note that for the symmetric case  $(C_{\text{tot}}^l, \mathcal{R}_{\text{tot}}^l) = (C_{\text{tot}}^r, \mathcal{R}_{\text{tot}}^r) = (C_{\text{tot}}, \mathcal{R}_{\text{tot}})$ . The insets of Figs. 7(a) and 7(b) show the corresponding temporal variation of  $C_{\text{tot}}$  and  $\mathcal{R}_{\text{tot}}$ , respectively. It is seen that  $C_{\text{tot}}$  increases with time as the amount of precipitation increases with time, see Fig. 2, while  $\mathcal{R}_{\text{tot}}$  decreases with time. However,  $C_{\text{tot}}$  and  $\mathcal{R}_{\text{tot}}$  are quite insensitive to changes in  $\delta_c$ .

#### IV. PARAMETRIC STUDY

As discussed in Sec. III, the nondimensional parameters, the change of which keeps fingering the same whether  $A$  invades  $B$  or vice versa, are the log-mobility ratio  $R$ , the Damköhler number  $D_a$ , and the diffusivity ratio  $\delta_c$ . This is due to the fact that they keep the underlying RD concentration profiles symmetric with regard to the initial contact position between the  $A$  and  $B$  solutions, see Fig. 3. The parameters that induce, on the contrary, an asymmetry are the initial concentration ratio  $\phi$  and the diffusivity ratio  $\delta_b$  of the reactant  $B$  when their value differs from 1. A different fingering dynamics is

then expected whether  $A$  is injected into  $B$  or vice versa. In this section we characterize the precipitation-driven fingering dynamics when varying these various parameters.

##### A. Effect of mobility ratio $R$ and Damköhler number $D_a$

As the log-mobility ratio  $R$  increases, the system becomes more unstable, producing more intense and expanded precipitate fingering patterns. This can be understood by the fact that, as  $R$  increases, the amplitude of the minimum of permeability increases [cf. (6)], which makes the system more unstable. As the effect of the Damköhler number  $D_a$  is concerned, we note that the fingering patterns are observed earlier when  $D_a$  is increased because the reaction time is then decreased with respect to the hydrodynamic time. This implies a larger production of the precipitate  $C$  in the reactive zone for a given time, leading to a favorable condition for precipitation fingering.

##### B. Effect of initial concentration ratio $\phi$

Let us now analyze the effect of changes in the initial concentration ratio  $\phi$  on fingering. Figure 8 shows the product concentration for  $\phi = 1, 1.5, 2.0$ , and  $2.5$ . The fingering patterns are the same in both reactive zones for  $\phi = 1$ , see Fig. 8(a), while for  $\phi \neq 1$  they differ whether  $A$  displaces  $B$  (left interface) or  $B$  invades  $A$  (right interface), see Figs. 8(b)–8(d). With increasing  $\phi$ , the fingering patterns of the left reactive zone become more regular, straight, and less interactive while those of the right reactive zone feature more splitting and merging [see the Supplemental Material for a movie of Fig. 8(d) [50]].

The origin of such an asymmetry of fingering patterns can be explained on the basis of the corresponding RD profiles of concentration and permeability, as shown in Fig. 9. If  $\phi > 1$ , then the reaction-diffusion front moves in time from the higher-concentrated region of  $B$  to the lower-concentrated zone containing  $A$ . The profile of the precipitate  $C$  is therefore asymmetric with a steeper gradient in the  $B$ -rich zone. The corresponding permeability profile, shown in Fig. 9(b), has thus

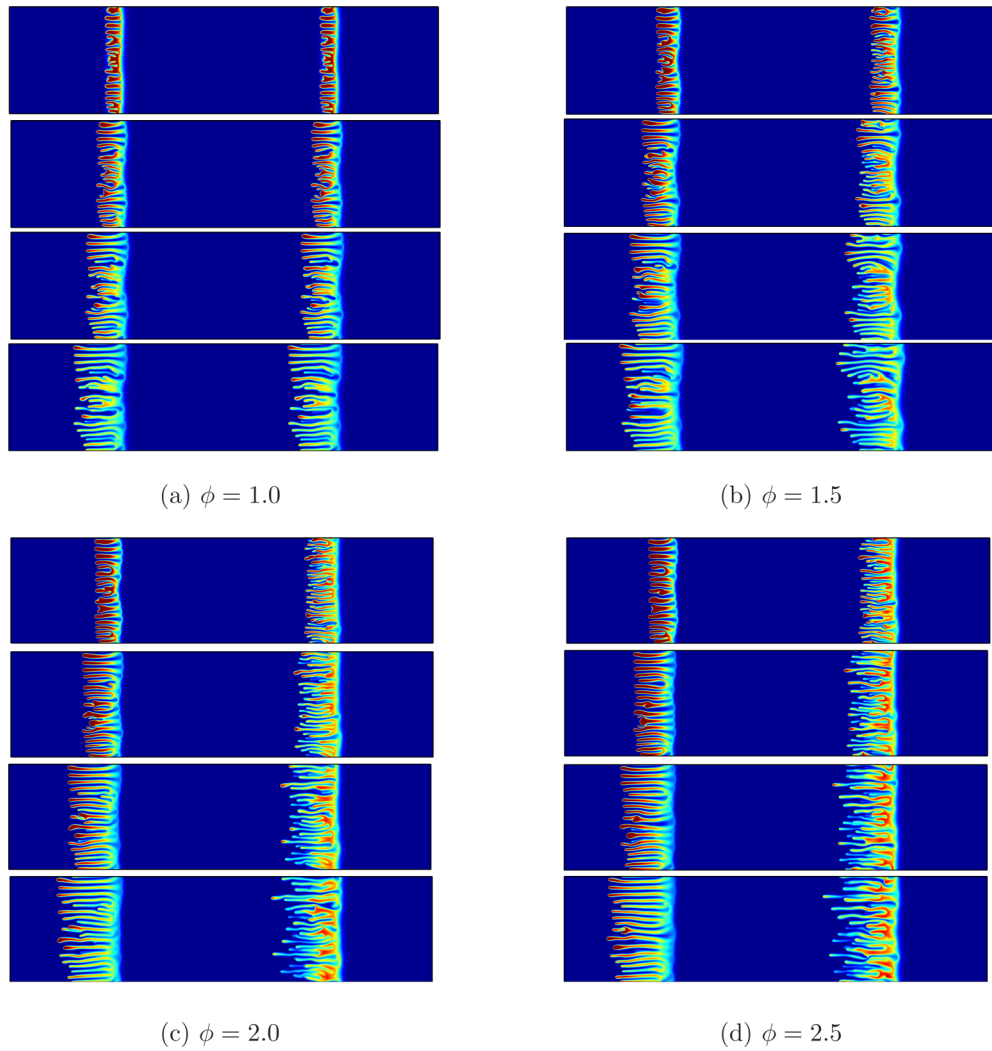


FIG. 8. Asymmetric fingering: Comparison of the product concentration for various values of  $\phi$ : (a) 1.0, (b) 1.5, (c) 2.0, and (d) 2.5 at time  $t = 40, 50, 60,$  and  $70$  (from top to bottom). Other parameters are the same as Fig. 2.

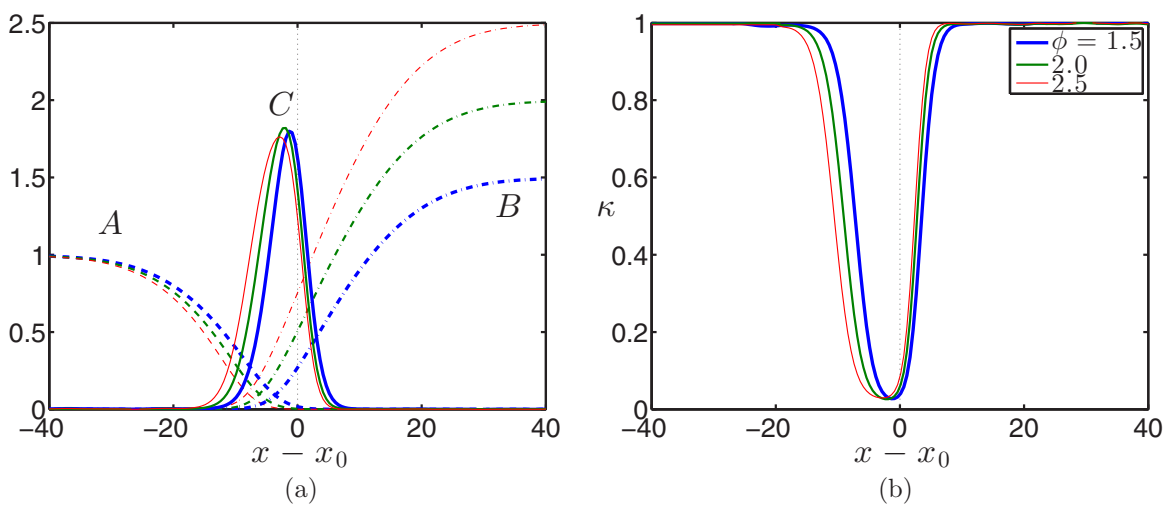


FIG. 9. Asymptotic RD profiles for (a) concentrations and (b) permeability for  $\phi$ : 1.5 (thickest blue line), 2.0 (thicker green line), and 2.5 (thick red line). The dashed, dash-dotted, and solid lines represent the concentrations of  $A$ ,  $B$ , and  $C$ , respectively. The initial location at  $x = x_l = x_r = x_0$  corresponds here to the black dotted line at origin. The other parameters are the same as those of Fig. 8.

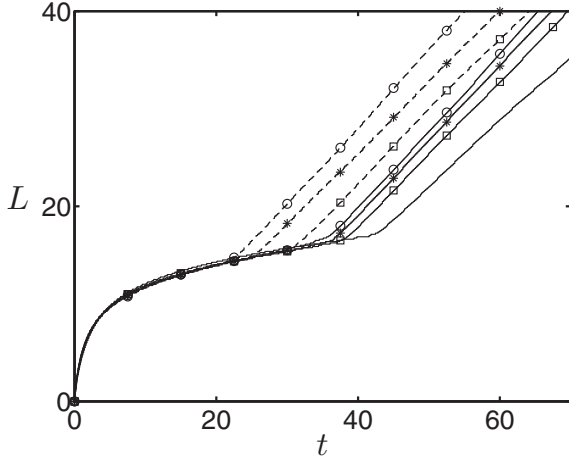


FIG. 10. Temporal variation of the mixing length for various values of  $\phi$ : 1.0 (solid line), 1.5 (square), 2.0 (star), and 2.5 (circle). All solid and dashed lines represent the left and right reactive zones, respectively. The other parameters are the same as those of Fig. 2.

also a steeper gradient  $d\kappa/dx$  in the  $B$ -rich part. Hence if  $B$  displaces  $A$ , then the corresponding unfavorable mobility profile is steeper than if  $A$  invades  $B$ , which explains the difference in patterns, as seen on Fig. 8. We also observe that, when increasing  $\phi$ , the gradient  $d\kappa/dx$  increases. Consequently, the RDC system becomes more unstable with increasing  $\phi$ , see Fig. 8.

The asymmetric characteristics of fingering can also be traced in the variation of the mixing lengths for different  $\phi$  when comparing them with the reference case  $\phi = 1$ , as shown in Fig. 10. It is observed that the averaged concentration profiles of the product become asymmetric sooner with increasing  $\phi$  because the onset time  $t = t_b$  for the appearance of asymmetry decreases. Thus, for  $\phi > 1$ , (i)  $L$  increases with increasing  $\phi$  in the convective regime and (ii)  $L$  in the right reactive zone is greater than that of the left reactive zone. From these observations, we conclude that the system becomes more unstable with increasing  $\phi$  and that the fingering patterns

are more intense at the right reactive zone, where the more concentrated solution  $B$  invades  $A$ , than in the left zone.

In order to look further on the role of asymmetry, the temporal evolution of the first moment of the product concentration and reaction rate profiles are shown for different  $\phi$ , in Fig. 11. At the left reactive zone, the first moment of the product concentration ( $m_c$ ) and of the reaction rate ( $m_R$ ) move towards the negative direction and decrease sharply in the presence of fingering. For this reason, the deviation of  $m_c$  and  $m_R$  from the initial location increases in time. By comparing the main panels of Figs. 8(a) and 8(b), we see that the reaction rate and the concentration of fingering are larger in the back of the left reactive zone as compared to those at the right zone.

In contrast to the left reactive zone,  $m_c$  at the right reactive zone moves first towards the positive direction until fingering appears beyond which it moves towards the negative direction. This can be understood by the fact that the corresponding RD profiles around the interface initially located at  $x_r$  where  $B$  invades  $A$  are pushed towards the right reactive zone (or towards the lower concentration). In the presence of fingering,  $m_c$  at the left shifts more towards the negative direction than that of the right, see Fig. 11(a). Since  $m_c$  at the left zone deviates more from its initial location as compared to the right, fingers at the left zone (where  $A$  invades  $B$ ) cover a larger area towards the left than at the right reactive zone (where  $B$  pushes  $A$ ), see Figs. 8(b)–8(d). It is observed in Fig. 11(b) that  $m_R$  moves towards the negative (positive) direction for the left (right) reactive zone. For the left (right) reactive zone, an increased reaction rate is present at the back (front) of the fingering zone. The total production of concentration  $C_{tot}$  and total reaction rate  $\mathcal{R}_{tot}$  are more or less the same at both reactive zones, as shown in the insets of Figs. 11(a) and 11(b), respectively.

### C. Effect of diffusivity ratio $\delta_b$

Another parameter which affects the symmetry of RD concentration profile is  $\delta_b$ . Different panels of Fig. 12 show the product concentrations for various values of  $\delta_b$ . When  $\delta_b \neq 1$ , i.e.,  $D_A \neq D_B$ , the underlying RD profiles become asymmetric, see Fig. 13(b). When  $\delta_b < 1$ , the fastest diffusing

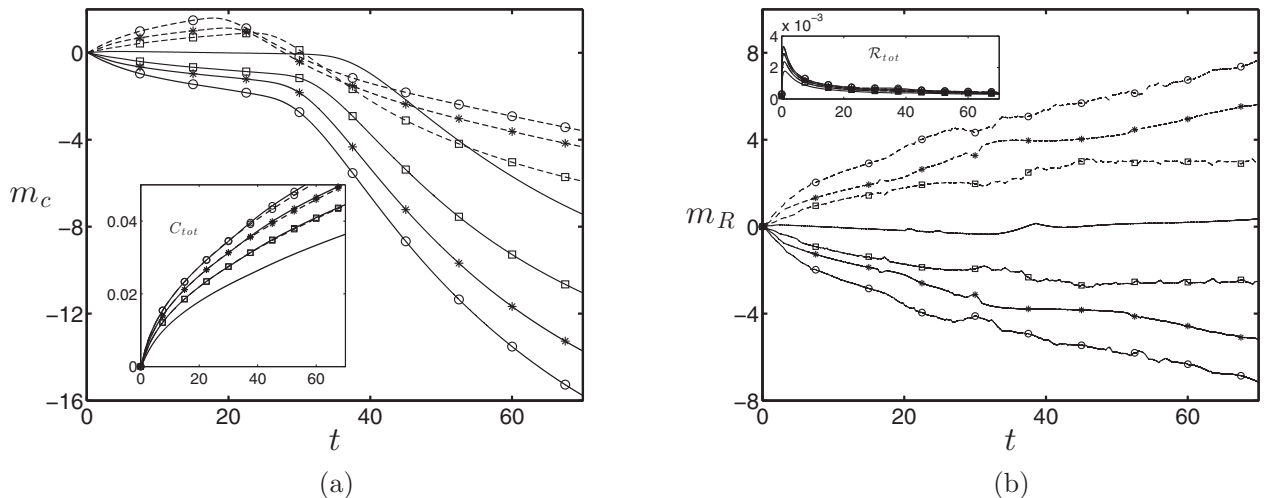


FIG. 11. Temporal variation of (a)  $m_c$  (main panel) and  $C_{tot}$  (inset) and (b)  $m_R$  (main panel) and  $\mathcal{R}_{tot}$  (inset). Other parameters along with convention of lines and symbols are the same as Fig. 10.

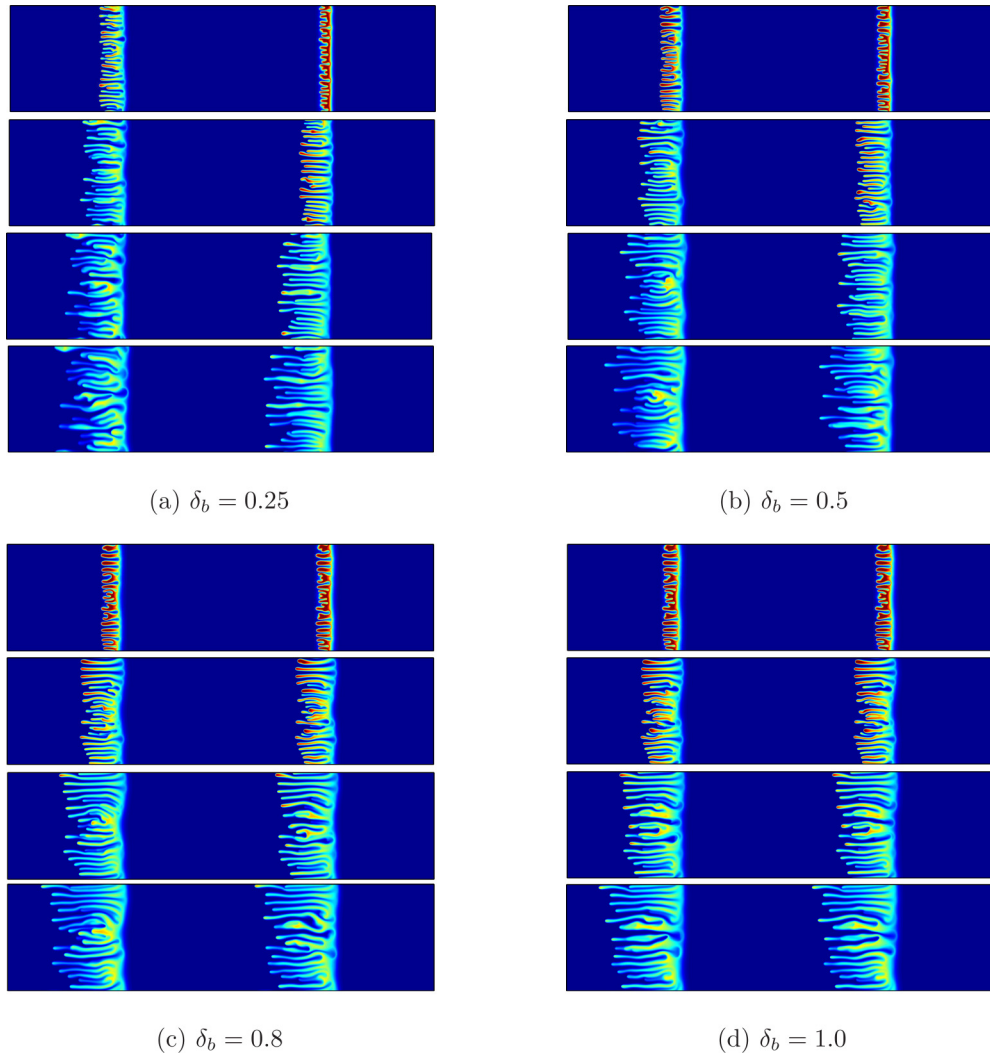


FIG. 12. Asymmetric fingering: Concentration of the product at  $t = 40, 60, 80,$  and  $100$  (from top to bottom) for  $\delta_b$ : (a) 0.25, (b) 0.5, (c) 0.8, and (d) 1.0. Other parameters are the same as in Fig. 2.

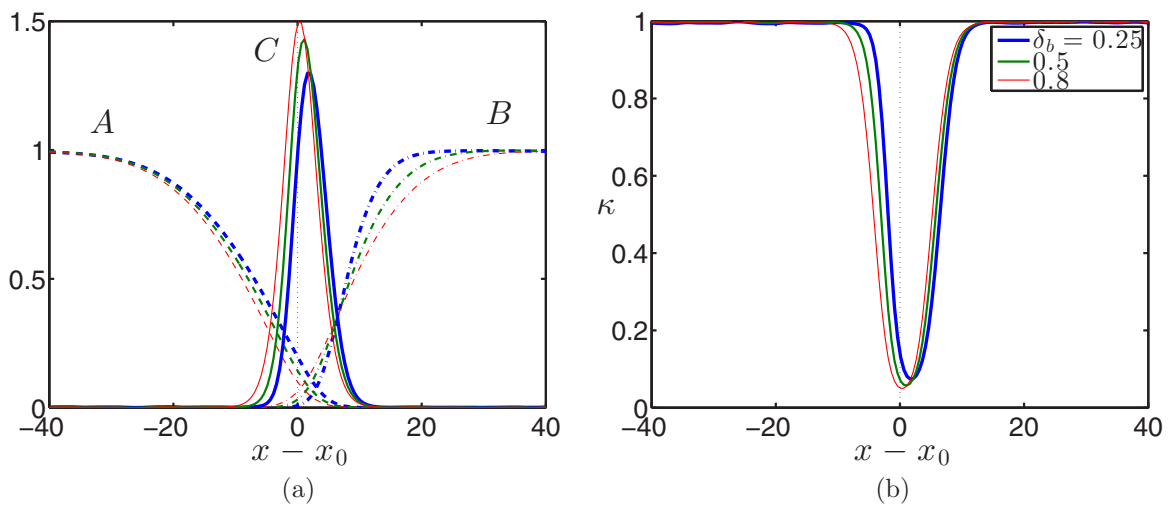


FIG. 13. Asymptotic transverse averaged RD profiles for (a) concentrations and (b) permeability for  $\delta_b$ : 0.25 (thickest blue line), 0.5 (thicker green line), and 0.8 (thick red line). The dashed, dash-dotted, and solid lines represent the concentrations of A, B, and C, respectively. The initial location at  $x = x_l = x_r = x_0$  corresponds here to the black dotted line at origin. The other parameters are the same as those of Fig. 12.

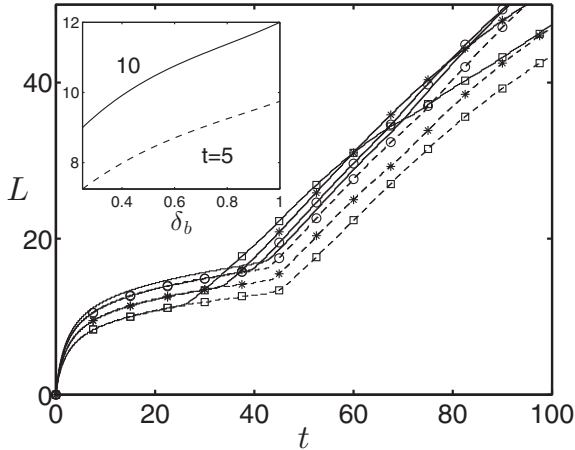


FIG. 14. Variation of the mixing length with time for  $\delta_b$ : 0.25 (square), 0.5 (star), and 0.8 (circle). The solid line without symbol represents  $\delta_b = 1$ . All solid and dashed lines represent left and right interfaces, respectively. Other parameters are the same as Fig. 2.

reactant  $A$  invades the slowest diffusing  $B$ , see Fig. 13(b), and an asymmetric permeability gradient develops which in turn gives rise to asymmetric fingering patterns in both reactive zones. It is clear from Fig. 13(b) that the unfavorable gradient  $d\kappa/dx < 0$  is sharper in the left reactive zone where the system is thus more unstable as seen in Fig. 12 [see the Supplemental Material for a movie of Fig. 12(a) [50]]. In addition, the intensity of fingering increases with decreasing  $\delta_b$ . This is due to the fact that  $d\kappa/dx$  increases with decreasing  $\delta_b$ , see Fig. 13(b).

Figure 14 shows that the corresponding mixing length significantly changes when  $\delta_B$  is varied. Initially the mixing length decreases when  $\delta_b$  decreases, however, in the convection-dominated regime, the instability sets in faster and the linear convective growth is steeper at the left interface when  $\delta_B$  decreases. This observation is consistent to what we see in Fig. 2, viz. the fingering patterns at the left reactive

zone are more unstable when we decrease  $\delta_b$ . The reverse is obtained at the right interface. In the inset of Fig. 14, we show the variation of  $L$  with  $\delta_b$  at time  $t = 5$  and 10 in the diffusion-dominated regime. It is observed that the diffusive mixing length is a monotonic increasing function of  $\delta_b$  [52,54], which means that, even in the case of no fingering, the zone of local precipitation increases with  $\delta_b$ . It is noted that, in the convection dominated regime, the mixing length at the left interface deviates in some cases from a linear growth later (see the  $\delta_b = 0.25$  and 0.5 curves in Fig. 14), probably due to merging between fingers due to transverse diffusion.

The effect of  $\delta_b$  on  $m_c$  and  $m_R$  are shown in Fig. 15. In the left reactive zone  $m_c$  first travels towards the right until convection dominates. However, in the right zone  $m_c$  always travels towards the left, Fig. 15(a). We can conclude that the precipitation fingering patterns cover a larger area in the right reactive zone. It is also verified that the absolute values of  $m_c$  and  $m_R$  increase and decrease with  $\delta_b$ , respectively. Subsequently,  $m_R$  shifts more towards the right (left) when  $A$  invades  $B$  ( $B$  invades  $A$ ) as we decrease  $\delta_b$ , as shown in Fig. 15(b).

V. COMPARISON WITH THE EXPERIMENTS

Our numerical results can be compared with the experiments reported by Nagatsu *et al.* [27]. As an example, the lowest panel of Fig. 12(a) compares the fingering at the left interface when the fast diffusing  $A$  invades the slow diffusing  $B$  ( $\delta_b = 0.25$ ), producing a solid product that barely diffuses ( $\delta_c = 0.01$ ) with the reverse case of  $B$  displacing  $A$  (right interface). This simulation is equivalent to the experimental case (shown in Fig. 1 of Ref. [27]) when  $A = \text{Fe}^{+3}$  is the displacing or displaced reactant in the experiment [27]. The diffusivity of the solution of  $\text{Fe}^{+3}$  is indeed larger than that of reactant  $B$  ( $= \text{K}_4[\text{Fe}(\text{CN})_6]$ ) i.e.,  $D_A > D_B$  ( $\delta_b < 1$ ). From Fig. 12, we see that the present simulation results are in qualitative agreement with the experiment. For the case when  $A$  pushes  $B$  (Fig. 12(a) left versus Fig. 1(e) in Ref. [27]),

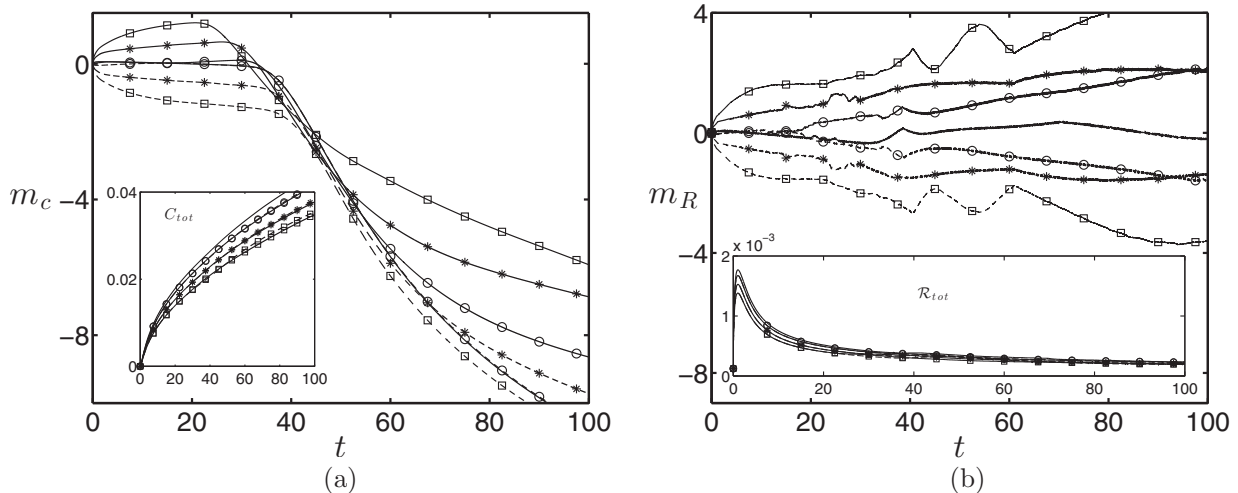


FIG. 15. Temporal variation of (a)  $m_c$  (main panel) and  $C_{tot}$  (inset) and (b)  $m_R$  (main panel) and  $\mathcal{R}_{tot}$  (inset). Other parameters along with convention of lines and symbols are the same as those of Fig. 14.

the precipitation fingers are more involved and uniformly distributed. On the contrary, when  $B$  pushes  $A$  (Fig. 12(a) right versus Fig. 1(f) in Ref. [27]), we see that the fingers are more concentrated at the right reactive zone. The present results are in good agreement with the experiments as well as previous simulations [27].

## VI. CONCLUSION

A simple  $A + B \rightarrow C$  precipitation reaction is able to change locally the permeability of a porous medium and trigger a fingering instability. We have numerically studied the properties of this precipitation-driven fingering when a solution of a reactant  $A$  displaces a solution of  $B$  to produce a solid product  $C$  in the miscible reactive zone. While mathematically the RDC model of precipitation-driven and that of reactive VF bear similarities, a specificity of the precipitation case is that the product  $C$  barely moves as it is a solid phase while, in reactive VF, the reactants  $A$ ,  $B$ , and product  $C$  have diffusion coefficients of the same order of magnitude. The model of precipitation-driven fingering needs thus to allow the possibility for  $D_C$ , the diffusion coefficient of solid  $C$  to tend to zero. We show that decreasing  $D_C$  destabilizes the system and that, in this limit of  $D_C \rightarrow 0$ , the onset time of precipitation fingering is much faster than that of reactive VF. Apart from this difference, precipitation fingering patterns are similar to their reactive VF equivalent if only the mobility is affected. In particular, they are similar whether  $A$  invades  $B$  or vice versa when the underlying RD concentration profiles are symmetric around the initial contact position. This is the case when the ratio of the initial concentrations and the diffusivity ratio of the reactants are equal to 1 ( $\phi = 1, \delta_b = 1$ ). Failing any of these conditions, when  $\phi \neq 1$  or  $\delta_b \neq 1$ , leads to asymmetric RD concentration profiles, subsequently leading to different precipitation patterns whether  $A$  displaces  $B$  or the reverse. Our results show that the system is more unstable with regard to precipitation fingering when the invading solution is either more concentrated or contains the fastest diffusing reactant.

Our results suggest that in order to develop given precipitate patterns by an  $A + B \rightarrow C$  precipitation reaction within a flow, the ratio of initial concentrations and diffusivity can be tuned to obtain a more or less important influence of the fingering patterns on the solid phase. For what concerns  $\text{CO}_2$  sequestration techniques, the present study provides a first mathematical framework in which to analyze the optimal conditions for safe and permanent mineralization of  $\text{CO}_2$  upon injection into aqueous solutions and precipitation with dissolved minerals.

The model studied here relies on simplifying assumptions such as the use of a constant porosity to focus on the effect of a concentration-dependent permeability only. This has allowed us to underline the mathematical analogy between reactive viscous fingering and precipitation- (and by extension dissolution) driven fingering. This is important because it suggests that all studies of effects that are known to influence viscous fingering (such as heterogeneities [42,43], velocity-dependent dispersion [44], or nonmonotonic mobility changes [55] to name a few) should straightforwardly be transposed to studies of channeling due to permeability changes. In

effect, however, fingering due to changes in the porous matrix by either dissolution or precipitation reactions can be more involved because of the feedback on porosity, too. It will be of interest to analyze if this feedback can lead to new properties of fingering not seen in viscous instabilities. In this regard, future work on precipitation-driven fingering should focus on using more realistic porosity and permeability dependence on concentration of precipitates to be able to tackle the situation in real porous media. This calls for additional experimental studies of such relations in model porous systems. Meanwhile, simpler experiments studying precipitation patterns can also be performed in Hele-Shaw cells [27–30]. In some cases, interplay with viscous fingering has been observed [31]. Progresses in modeling of such fingering dynamics in Hele-Shaw geometries should incorporate 3D effects in the gap of the cell [56,57] as well as viscous [30,31] or mechanical effects due to cohesive properties of the solid matrix [28].

## ACKNOWLEDGMENTS

We thank Y. Nagatsu, F. Brau, F. Haudin, M. Mishra, and B. Dice for fruitful discussions. P.S. is beneficiary of a mobility grant from the Belgian Federal Science Policy Office. P.S. acknowledges financial support from IIT Madras in the form of a New Faculty Initiation Grant (MAT/15-16/833/NFIG/PRIY), and A.D. acknowledges PRODEX for financial support.

## APPENDIX

The results obtained here can be compared with those discussed in Nagatsu *et al.* [27] modulo a change of variable. In dimensional form, our model is the same as given in Ref. [27]. However, Nagatsu *et al.*'s characteristic scales are based on  $D_C$ , the diffusion coefficient of the solid product. To allow us to tackle the  $\delta_c \rightarrow 0$  limit specific to precipitation more easily, we use here other characteristic scales based on  $D_A$ , the diffusion coefficient of the reactant A. To compare both approaches, the following relationship between parameters should be used:

$$\delta_c = \frac{1}{\delta_a^N}, \quad \delta_b = \frac{\delta_b^N}{\delta_a^N}, \quad D_a = D_a^N \delta_a^N, \quad \text{and} \\ \text{Pe}' \times \text{Pe} = \frac{1}{\delta_a^N} (\text{Pe}'^N \times \text{Pe}^N), \quad (\text{A1})$$

where the superscript  $N$  refers to the parameters used in Ref. [27]. For example, the parameters  $\delta_a^N = 20$ ,  $\delta_b^N = 5$ , and  $D_a^N = 1$  in Ref. [27] correspond to  $\delta_c = 0.05$ ,  $\delta_b = 0.25$ , and  $D_a = 20$  in the present model. If the dimensionless length and width in Ref. [27], for example, are set to  $(\text{Pe}'^N \times \text{Pe}^N) = (2048 \times 1024)$ , then in the present model these correspond to  $(\text{Pe}' \times \text{Pe}) = (102.5 \times 51.2)$ . Similarly, in the reverse case, parameters corresponding to Fig. 2 here, i.e.,  $\delta_c = 0.01, \delta_b = 1, D_a = 1$ , correspond to  $\delta_a^N = \delta_b^N = 100$  and  $D_a^N = 0.01$ , respectively.

- [1] S. Hill, Channeling in packed columns, *Chem. Eng. Sci.* **1**, 247 (1952).
- [2] R. A. Wooding and H. J. Morel-Seytoux, Multiphase fluid flow through porous media, *Annu. Rev. Fluid Mech.* **8**, 233 (1976).
- [3] D. Bensimon, L. P. Kadanoff, S. Liang, B. I. Shraiman, and C. Tang, Viscous flows in two dimensions, *Rev. Mod. Phys.* **58**, 977 (1986).
- [4] G. M. Homsy, Viscous fingering in porous media, *Annu. Rev. Fluid Mech.* **19**, 271 (1987).
- [5] S. Berg and H. Ott, Stability of CO<sub>2</sub>-brine immiscible displacement, *Int. J. Greenhouse Gas Control* **11**, 188 (2012).
- [6] S. R. Lunn and B. H. Kueper, Manipulation of density and viscosity for the optimization of DNAPL recovery by alcohol flooding, *J. Contam. Hydrol.* **38**, 427 (1999).
- [7] C. T. Tan and G. M. Homsy, Simulation of nonlinear viscous fingering in miscible displacement, *Phys. Fluids* **31**, 1330 (1988).
- [8] C. T. Tan and G. M. Homsy, Stability of miscible displacements in porous media: Rectilinear flow, *Phys. Fluids* **29**, 3549 (1986).
- [9] K. McCloud and J. Maher, Experimental perturbations to Saffman-Taylor flow, *Phys. Rep.* **260**, 139 (1995).
- [10] A. De Wit and G. M. Homsy, Viscous fingering in reaction-diffusion systems, *J. Chem. Phys.* **110**, 8663 (1999).
- [11] A. De Wit and G. M. Homsy, Nonlinear interactions of chemical reactions and viscous fingering in porous media, *Phys. Fluids* **11**, 949 (1999).
- [12] M. Jahoda and V. Hornof, Concentration profiles of reactant in a viscous finger formed during the interfacially reactive immiscible displacements in porous media, *Powder Technol.* **110**, 253 (2000).
- [13] Y. Nagatsu and T. Ueda, Effects of reactant concentrations on reactive miscible viscous fingering, *AIChE J.* **47**, 1711 (2001).
- [14] Y. Nagatsu, K. Matsuda, Y. Kato, and Y. Tada, Experimental study on miscible viscous fingering involving viscosity changes induced by variations in chemical species concentrations due to chemical reactions, *J. Fluid Mech.* **571**, 475 (2007).
- [15] T. Gérard and A. De Wit, Miscible viscous fingering induced by a simple  $A + B \rightarrow C$  chemical reaction, *Phys. Rev. E* **79**, 016308 (2009).
- [16] S. H. Hejazi, P. M. J. Trevelyan, J. Azaiez, and A. De Wit, Viscous fingering of a miscible reactive  $A + B \rightarrow C$  interface: A linear stability analysis, *J. Fluid Mech.* **652**, 501 (2010).
- [17] S. H. Hejazi and J. Azaiez, Hydrodynamic instability in the transport of miscible reactive slices through porous media, *Phys. Rev. E* **81**, 056321 (2010).
- [18] Y. Nagatsu and A. De Wit, Viscous fingering of a miscible reactive  $A + B \rightarrow C$  interface for an infinitely fast chemical reaction: Nonlinear simulations, *Phys. Fluids* **23**, 043103 (2011).
- [19] L. A. Riolfo, Y. Nagatsu, S. Iwata, R. Maes, P. M. J. Trevelyan, and A. De Wit, Experimental evidence of reaction-driven miscible viscous fingering, *Phys. Rev. E* **85**, 015304 (2012).
- [20] S. H. Hejazi and J. Azaiez, Nonlinear simulation of transverse flow interactions with chemically driven convective mixing in porous media, *Water Resour. Res.* **49**, 4607 (2013).
- [21] J. Chadam, D. Hoff, E. Merino, P. Ortoleva, and A. Sen, Reactive infiltration instabilities, *IMA J. Appl. Math.* **36**, 207 (1986).
- [22] G. Daccord, Chemical Dissolution of a Porous Medium by a Reactive Fluid, *Phys. Rev. Lett.* **58**, 479 (1987).
- [23] J. D. Sherwood, Stability of a plane reaction front in a porous medium, *Chem. Eng. Sci.* **42**, 1823 (1987).
- [24] E. J. Hinch and B. S. Bhatt, Stability of an acid front moving through porous rock, *J. Fluid Mech.* **212**, 279 (1990).
- [25] P. Szymczak and A. J. C. Ladd, Interacting length scales in the reactive-infiltration instability, *Geophys. Res. Lett.* **40**, 3036 (2013).
- [26] P. Szymczak and A. J. C. Ladd, Reactive-infiltration instabilities in rocks. Part 2. Dissolution of a porous matrix, *J. Fluid Mech.* **738**, 591 (2014).
- [27] Y. Nagatsu, Y. Ishii, Y. Tada, and A. De Wit, Hydrodynamic Fingering Instability Induced by a Precipitation Reaction, *Phys. Rev. Lett.* **113**, 024502 (2014).
- [28] F. Haudin, J. H. E. Cartwright, F. Brau, and A. De Wit, Spiral precipitation patterns in confined chemical gardens, *Proc. Natl. Acad. Sci. USA* **111**, 17363 (2014).
- [29] F. Haudin, V. Brasiliense, J. H. E. Cartwright, F. Brau, and A. De Wit, Genericity of confined chemical garden patterns with regard to changes in the reactants, *Phys. Chem. Chem. Phys.* **17**, 12804 (2015).
- [30] F. Haudin, J. H. E. Cartwright, and A. De Wit, Direct and reverse chemical garden patterns grown upon injection in confined geometries, *J. Phys. Chem. C* **119**, 15067 (2015).
- [31] F. Haudin and A. De Wit, Patterns due to an interplay between viscous and precipitation-driven fingering, *Phys. Fluids* **27**, 113101 (2015).
- [32] C. Zhang, K. Dehoff, N. Hess, M. Oostrom, T. Wietsma, A. J. Valocchi, B. W. Fouke, and C. J. Werth, Pore-scale study of transverse mixing induced CaCO<sub>3</sub> precipitation and permeability reduction in a model subsurface sedimentary system, *Environ. Sci. Technol.* **44**, 7833 (2010).
- [33] C. Zhang, M. Oostrom, J. W. Grate, T. W. Wietsma, and M. G. Warner, Liquid CO<sub>2</sub> displacement of water in a dual-permeability pore network micromodel, *Environ. Sci. Technol.* **45**, 7581 (2011).
- [34] Y. Nagatsu, S.-K. Bae, Y. Kato, and Y. Tada, Miscible viscous fingering with a chemical reaction involving precipitation, *Phys. Rev. E* **77**, 067302 (2008).
- [35] Y. Bernabé, U. Mok, and B. Evans, Permeability-porosity relationships in rocks subjected to various evolution processes, *Pure Appl. Geophys.* **160**, 937 (2003).
- [36] B. Lamy-Chappuis, D. Angus, Q. Fisher, C. Grattoni, and B. W. D. Yardley, Rapid porosity and permeability changes of calcareous sandstone due to CO<sub>2</sub>-enriched brine injection, *Geophys. Res. Lett.* **41**, 399 (2013).
- [37] L. Luquot and P. Gouze, Experimental determination of porosity and permeability changes induced by injection of CO<sub>2</sub> into carbonate rocks, *Chem. Geol.* **265**, 148 (2009).
- [38] P. Gouze and L. Luquot, X-ray microtomography characterization of porosity, permeability and reactive surface changes during dissolution, *J. Contam. Hydrol.* **120-121**, 45 (2011).
- [39] J. Verdon and A. Woods, Gravity-driven reacting flows in a confined porous aquifer, *J. Fluid Mech.* **588**, 29 (2007).
- [40] P. Szymczak and A. J. C. Ladd, Instabilities in the dissolution of a porous matrix, *Geophys. Res. Lett.* **38**, L07403 (2011).
- [41] L. Ritchie and D. Pritchard, Natural convection and the evolution of a reactive porous medium, *J. Fluid Mech.* **673**, 286 (2011).
- [42] C. Tan and G. M. Homsy, Viscous fingering with permeability heterogeneity, *Phys. Fluids A* **4**, 1099 (1992).
- [43] A. De Wit and G. M. Homsy, Viscous fingering in periodically heterogeneous porous media. ii: Numerical simulations, *J. Chem. Phys.* **107**, 9619 (1997).

- [44] W. Zimmerman and G. M. Homsy, Viscous fingering in miscible displacements: Unification of effects of viscosity contrast, anisotropic dispersion, and velocity dependence of dispersion on nonlinear finger propagation, *Phys. Fluids A* **4**, 2348 (1992).
- [45] S. Pramanik and M. Mishra, Effect of Péclet number on miscible rectilinear displacement in a Hele-Shaw cell, *Phys. Rev. E* **91**, 033006 (2015).
- [46] L. Cueto-Felgueroso and R. Juanes, A phase-field model of two-phase Hele-Shaw flow, *J. Fluid Mech.* **758**, 522 (2014).
- [47] C. Canuto, M. Y. Hussani, A. Quarteroni, and T. A. Zang, *Spectral Methods in Fluid Dynamics* (Springer, Berlin, 1988).
- [48] B. Fornberg, *A Practical Guide to Pseudospectral Methods*, Cambridge Monographs on Applied and Computational Mathematics (Cambridge University Press, Cambridge, 1998).
- [49] D. Gottlieb and E. Tadmor, The CFL condition for spectral approximations to hyperbolic initial-boundary value problems, *Math. Comp.* **56**, 565 (1991).
- [50] See Supplemental Material at <http://link.aps.org/supplemental/10.1103/PhysRevE.93.023103> for movies of the precipitation dynamics with parameters: (1)  $\delta_c = 0.01$ ,  $\delta_b = \phi = 1$ ,  $R = 2$ ,  $D_a = 1$  (Fig. 1), (2)  $\delta_c = 0.01$ ,  $\delta_b = 1$ ,  $\phi = 2.5$ ,  $R = 2$ ,  $D_a = 1$  (Fig. 8(d)), and  $\delta_c = 0.01$ ,  $\delta_b = 0.25$ ,  $\phi = 1$ ,  $R = 2$ ,  $D_a = 1$  (Fig. 12(a)).
- [51] M. Mishra, M. Martin, and A. De Wit, Differences in miscible viscous fingering of finite width slices with positive or negative log-mobility ratio, *Phys. Rev. E* **78**, 066306 (2008).
- [52] L. Gálfi and Z. Rácz, Properties of the reaction front in an  $A + B \rightarrow C$  type reaction-diffusion process, *Phys. Rev. A* **38**, 3151 (1988).
- [53] A. De Wit, Y. Bertho, and M. Martin, Viscous fingering of miscible slices, *Phys. Fluids* **17**, 054114 (2005).
- [54] Z. Koza, The long-time behavior of initially separated  $A + B \rightarrow 0$  reaction-diffusion systems with arbitrary diffusion constants, *J. Stat. Phys.* **85**, 179 (1996).
- [55] O. Manickam and G. M. Homsy, Simulation of viscous fingering in miscible displacements with nonmonotonic viscosity profiles, *Phys. Fluids* **6**, 95 (1994).
- [56] F. Haudin, L. A. Riolfo, B. Knaepen, G. M. Homsy, and A. De Wit, Experimental study of a buoyancy-driven instability of a miscible horizontal displacement in a Hele-Shaw cell, *Phys. Fluids* **26**, 044102 (2014).
- [57] N. Rakotomalala, D. Salin, and P. Watzky, Miscible displacement between two parallel plates: BGK lattice gas simulations, *J. Fluid Mech.* **338**, 277 (1997).